Amygdala neuronal ensembles dynamically encode behavioral states

Jan Gründemann[1,*,#], Yael Bitterman[1,*], Tingjia Lu[1], Sabine Krabbe[1], Benjamin F. Grewe[2,3], Mark J. Schnitzer[4] & Andreas Lüthi[1,5]

[1]Friedrich Miescher Institute for Biomedical Research, Maulbeerstrasse 66, Basel, Switzerland,
[2]Institute of Neuroinformatics, University and ETH Zürich, Winterthurerstrasse 190, Zürich, Switzerland,
[3]Dept. of Electrical Engineering and Information Technology, ETH Zurich,
[4]Howard Hughes Medical Institute, CNC Program, James H. Clark Center Biomedical Engineering and Sciences, Stanford University, Stanford, USA,
[5]University of Basel, 4000 Basel, Switzerland,
*these authors contributed equally
[#]present address: University of Basel, Department of Biomedicine, Klingelbergstrasse 50-70, Basel, Switzerland
Contact: andreas.luthi@fmi.ch, jan.grundemann@unibas.ch

Abstract

Internal states, including affective or homeostatic states, are important behavioral motivators. The amygdala is a key brain region involved in the regulation of motivated behaviors, yet how distinct internal states are represented in amygdala circuits is not known. Here, by imaging somatic neural calcium dynamics in freely moving mice, we demonstrate that changes in the relative activity levels of two major, non-overlapping populations of principal neurons in the basal nucleus of the amygdala (BA) predict switches between exploratory and anxiety-like or defensive behavioral states across different environments. Moreover, we found that the amygdala widely broadcasts internal state information via several output pathways to larger brain networks, and that sensory responses in the BA were not correlated with behavioral states. Our data indicate that the brain processes external stimuli and internal states in an orthogonal manner, which may facilitate rapid and flexible selection of appropriate, state-dependent behavioral responses.

Main

Sensory processing and behavior are regulated by internal states, which mediate state-dependent adaptations of perception and the selection of appropriate behavioral outputs (e.g. flight vs. foraging) to promote an animal's survival[1]. Homeostatic states such as hunger and thirst, or affective states induced by aversive or appetitive experience are associated with behavioral, perceptual, autonomic and hormonal read-outs. For example, predator exposure elicits a defensive state in rodents, which is manifested by increased cortisol levels and analgesia[2–4], arousal and sensorymotor-gating changes[4–6] as well as (long lasting) anxiety-like behaviors[7,8]. The physiological and behavioral outputs (e.g. context exploration or freezing in mice) may thus act as a trackable proxy for internal states (e.g. low-anxiety vs. defensive state), that can then be tested for their generality across contexts and paradigms.

Classical and recent studies identified state-related brain areas and neural circuits[9] via electrical and optogentic stimulation, which lead to fast shifts in affective and defensive behaviors, foraging drives, feeding behavior and systemic hormonal levels[10–17]. This suggests that internal states are defined by a dynamic interplay involving specific patterns of neuronal activity across large brain networks[18], yet these neuronal representations are unknown and we are only starting to identify the neuronal circuit basis of internal states[19–21].

The basolateral amygdala (BLA) and particularly its basal nucleus (BA), a brain hub for the regulation of affective, homeostatic and social behaviors, are functionally linked to all above-mentioned levels via direct and indirect reciprocal neuronal circuits; e.g. to motor pathways[22] driving specific behavioral output, to thalamic and cortical sensory areas implicated in the processing of outcome-prediciting stimuli[23,24], as well as to brain centers that sense and regulate behaviorally-relevant hormones and neuromodulators[25]. Much research on amygdala function has involved the framework of appetitive and aversive Pavlovian conditioning[26–29], leading to the identification of the specific circuit elements underlying associative plasticity in aversive conditioning[30–32] as well as the response patterns of amygdala neuronal ensembles representing conditioned and unconditioned stimuli[33]. While these works thoroughly characterize the amygdala activity that is learned and temporally locked to experimentally controlled events, we only have a rudimentary understanding of how the activity of amygdala neurons relates to self-paced behaviors like foraging, risk assessment, or place avoidance[34,35]. These behaviors are strongly driven by internal states, such as anxiety[36], and may therefore serve as their external manifestation and read-out.

To address how internal states are represented on the level of distributed activity in either the whole population of amygdala neurons[18] or dedicated

functional state-ensembles, we performed deep brain calcium imaging of large populations of BA principal neurons (PNs) using a miniaturized microscope[33,37] in animals that engage in a series of behavioral paradigms, including the exploration of environments traditionally associated with changing levels of anxiety as well as Pavlovian fear conditioning. By following large neuronal populations longitudinally across several days and paradigms (**Extended Data Fig. 1**), we identify a trackable neuronal population signature of internal states in the BA, which reoccurs upon diverse behaviors. These state signatures are represented by fixed, functional neuronal ensembles, broadcast to multiple downstream brain areas and do not correlate with sensory input-driven BA population activity, indicating that behaviorally relevant internal states and sensory inputs seem to be encoded in an orthogonal manner.

Amygdala activity during open field exploration

To investigate general principles of BA population coding, we used a miniature fluorescence microscope (**Fig. 1a, Extended Data Fig. 1a-d**) to track the relative changes in Ca^{2+} fluorescence in large populations of BA PNs (CaMKII-positive as well as projection-specific PN populations, **Extended Data Fig. 6**) in freely moving mice across three consecutive behavioral paradigms (open field test, OF; elevated plus maze test, EPM; auditory fear conditioning, FC; **Fig. 1b; Fig. 5a, Extended Data Fig. 1**). As previously described[38–41], mice spent most time in the periphery of the OF (**Fig. 1d,** periphery: 76 ± 3%, center: 24 ± 3%, $P < 0.0001$, Wilcoxon matched-pairs signed rank test, N = 25 mice). Nevertheless, mice typically exhibited pronounced exploratory behavior in the OF (**Fig. 1g, Extended Data Fig. 2h**). They covered large distances (45 ± 2 m in ca. 10 min, N = 25 mice) (**Fig. 1c**) and ventured out of the corners along the walls (time in corners: 34 ± 2%, time at walls: 42 ± 1%, $P < 0.01$, Wilcoxon matched-pairs signed rank test, N = 25 mice) and into the center (**Fig. 1d**).

Ca^{2+} activity of BA CaMKII-positive PNs (133 ± 6 neurons / animal, N = 9 mice) was tracked throughout OF exploration using miniaturized microscopy (**Fig. 1a, Extended Data Fig. 1**). During the OF test, BA neurons exhibited diverse activity patterns with burst-like as well as slow changes of Ca^{2+} fluorescence (**Fig. 1h**). The average spatial response patterns of individual BA neurons in the OF arena ranged from seemingly non-specific to area-biased activity, with relatively more activity in the corners (corner-modulated cells) or the center (center-modulated cells) of the OF (**Fig. 1i**). The area-bias was quantified by the differential Ca^{2+} activity between corners and centers (area score, see Methods), and neurons with scores exceeding a selected threshold were defined as area-modulated (total area modulated: 28 ± 5%) (**Fig. 2a,b**). The area score distribution based on differential activity in corners vs. centers was larger than area scores based on neutral divisions of the open field (e.g. left vs. right, top vs. bottom, **Extended Data Fig. 2a**). Furthermore, a substantial fraction of corner vs. center-based area scores was outside of the 95% confidence interval of the left vs. right and top vs. bottom (17% and 21%, respectively) distribution, indicating that corner/center-related activity is significantly different from random spatial activity changes in the open field. The total BA population did not exhibit a specific quantitative bias towards more activity in the corners or in the center (corners: 13 ± 3% of BA PNs/animal; center: 15 ± 3%; $P = 0.641$, Wilcoxon matched-pairs signed rank test) (**Fig. 2c**). Corner-modulated and center-modulated neurons were spatially intermingled in the BA and showed no apparent local clustering (**Fig. 2d,e, Extended Data Fig. 2b**).

To examine neuronal dynamics during an animal's transition from the OF center into a corner, and vice versa, we averaged neuronal Ca^{2+} responses according to directionality and to the time point when the animal crossed the center/corner boundary. This analysis revealed that a large group of BA neurons was either activated (27 ± 4%, ensemble 1) or inhibited (29 ± 4%, ensemble 2, $P = 0.641$, Wilcoxon matched-pairs signed rank test, see Methods for details on cluster based analysis of relative changes in Ca^{2+} fluorescence) upon spatial relocation (**Fig. 2f,g**). Interestingly, the sign of the response of the respective BA ensemble was inverted when the animal exited the corner area, albeit similar speed profiles for both transitions (**Fig. 2g**). By and large, ensemble 1 cells overlapped with corner-modulated cells, whereas ensemble 2 cells corresponded to center-modulated cells (**Extended Data Fig. 2e-g**). The activity patterns of corner- and center-modulated cells were linked to the spatial location or the transition therein and did not depend on differences in average corner and center movement (**Extended Data Fig. 2h**), general speed correlations on the single cell level (**Extended Data Fig. 2i**), or correlations of neuronal activity with instantaneous changes in speed (**Fig. 2g, Extended Data Fig. 2j**).

Given the strong area-modulation of the neuronal responses, we next trained a support vector machine classifier (see Methods) to test if corner or center locations of the animal can be accurately predicted solely based on BA population activity. Indeed, the classifier reached high decoding accuracies of 86 ± 2%, whilst decoder performance dropped if the neuronal data was temporally shuffled (46 ± 4%, $P = 0.004$, Wilcoxon matched-pairs signed rank test) (**Fig. 2h**) or circularly shifted to control for local structures in the behavioral and neuronal data (**Extended Data Fig. 2c**, see also Methods).

Taken together, this data shows that, during the OF exploration, a large fraction of BA neurons conveys area-modulated information about an animal's corner

or center location; areas which are typically considered to reflect different internal states with regard to the animal's anxiety or stress levels[39,42–44].

Amygdala encoding of elevated plus maze exploration

To investigate whether general principles of BA population coding apply to exploratory behavior across different contexts, we imaged the same BA PNs during EPM exploration (**Fig. 1b, Extended Data Fig. 1e**). In keeping with the OF test, mice spent more time in the closed arms of the EPM (closed: 81 ± 2%). Typically, one of the closed arms, the preferred home base arm, was substantially more frequented (**Extended Data Fig. 3a**). Similar to our observations in the OF test, mice also exhibited exploratory behavior on the EPM. They ventured out of the closed arms into the center (relative time spent: 13 ± 2%) or onto the open arms (6 ± 1%, $P < 0.0001$, Friedman test) (**Fig. 1e**). Furthermore, the animals performed so-called head dips, marked by brief periods of visual investigation over the edge of the EPM open arms (**Fig. 1f**).

Next, we asked whether the area-modulated responses of BA PNs which we observed in the OF would generalize to the EPM. Specifically, we hypothesized enclosed, potentially safe areas are similarly represented between the two paradigms, such that corner-modulated cells might be more active during an animal's stay in the closed arm of the EPM, whereas center-modulated cells might show higher activity levels during open arm exploration. Surprisingly, average activity of corner-modulated cells was reduced in the preferred closed arm (mean z-score: -0.22 ± 0.03, N = 9 animals) (**Fig. 3b,e**), whereas center-modulated cells exhibited increased activity in the preferred closed arm (mean z-score: 0.15 ± 0.04, $P < 0.01$, Wilcoxon matched-pairs signed rank test) (**Fig. 3c,e**). Once the animal started to venture out of its preferred closed arm to explore the EPM, average activity of corner- and center-modulated cells reversed such that corner-modulated cells increased their Ca^{2+} fluorescence in the center (Δz-score: 0.246 ± 0.04), less frequented closed arm (Δz-score: 0.262 ± 0.04) or open arms (Δz-score: 0.222 ± 0.03), and vice-versa for center-modulated cells (Δz-score for center = -0.177 ± 0.04, closed-avoided = -0.183 ± 0.05, open = -0.156 ± 0.05; all $P < 0.01$, Wilcoxon matched-pairs signed rank test) (**Fig. 3d-f**). This suggests that the activity of corner-modulated cells correlates with exploration of the non-preferred closed and open arms of the EPM. Consistent with this notion, the animals' behavior in the OF corners was not passive, but rather characterized by constant activity, exploration and rearing (**Extended Data Fig. 2h and 3b**).

To test this idea further, we analyzed activity of corner- and center-modulated cells during open arm head dips, a classic exploratory, low anxiety behavior[45]. On average, the animals performed 18 ± 2 head dips per EPM session. As expected, during head dips, corner-modulated cells were strongly activated (z-score: 0.28 ± 0.04) whereas center-modulated cells were inhibited (z-score: -0.23 ± 0.08, $P < 0.01$, Wilcoxon matched-pairs signed rank test) (**Fig. 3g-i**). These data demonstrate that the opposing activation pattern of corner- and center-modulated cell ensembles is preserved during head dips, an alternative, stationary exploratory behavior. Together, these data indicate that two large, non-overlapping functional ensembles of BA PNs signal fundamentally distinct states characterized by the presence or absence of exploratory behavior across different paradigms.

Consistent encoding of behavioral states in amygdala ensembles

Next, we asked how behavioral states and the transitions between them are encoded on the neuronal population level. To follow the modulation of BA ensemble activity across different states and behavioral paradigms, we used open field area transitions, reminiscient of state transitions, and clustered the neurons according to their OF corner entry responses into activated (ensemble 1, 27 ± 4% of all neurons), neutral (44 ± 3%) or inhibited (ensemble 2, 29 ± 4%) neurons (**Fig. 4a**, see also **Fig. 2g**). On average, the activated and inhibited ensembles showed inverted relative changes in Ca^{2+} fluorescence upon corner exit (**Fig. 4a-c, Fig. 2g**). We next analysed the activity of these three ensembles across different behaviors using the same cluster partition and cell IDs. Indeed, consistent with the ideas that ensemble 1 neurons encode a general state associated with exploratory behavior across animals, ensemble 1 cells were not only activated upon OF corner entries, but also upon open arm head dip behavior (**Fig. 4a-c, see also Fig. 3 g-i**). In contrast, ensemble 2 neurons exhibited the inverse pattern of activity modulation (**Fig. 4a-c**). Notably, when extending this analysis to freezing behavior, a defensive behavior induced by auditory fear conditioning, we found that ensemble 1 and ensemble 2 neurons showed opposite activity changes when animals transitioned into a high fear, freezing state and upon termination of freezing (**Fig. 4a**, for details see Methods).

While ensemble responses were averaged across many neurons (44 ± 3 cells / cluster), a similar result was obtained for single neuron responses. For example, population response correlations between corner entry and corner exit were highly negative ($R = -0.84$, $P < 0.001$) (**Fig. 4d**). Overall, population level correlations between corner entry, freezing end and head dips were highly positive, whereas the neuronal correlation of these behaviors was inversely correlated with freezing start and corner exit behaviors (**Fig. 4e**). These correlations were independent of the behavioral session (i.e. freezing during habituation or extinction 1 and 2) (**Fig. 4e**).

Together, these data reveal the population level encoding of behavioral states by large, antagonistic ensembles of BA neurons, which switch their activity patterns upon opposing exploratory and anxiety-like or defensive behavioral states.

Orthogonal behavioral and sensory coding in BA neuronal ensembles.

Next, we tested how the population coding of behavioral states in BA neurons intersects with sensory coding during the acquisition and extinction of classical Pavlovian fear conditioning. During conditioning, we paired a previously neutral pure tone (conditioned stimulus, CS+, 75 dB pure tone) with a mild electrical foot shock (unconditioned stimulus, US, 2 s, 0.65 mA AC, see Methods). After conditioning, the animals showed increased freezing responses towards the CS+, which was extinguished by a repetitive re-exposure of the CS+ (**Fig. 5a**). BA neurons were ca. two times more likely to respond to the US (57 ± 3% of all neurons including excitatory and inhibitory responses, N = 9 animals) (**Fig. 5c,f**) than to the CSs (30 ± 3% of all neurons, P = 0.004, N = 9 animals; Wilcoxon matched-pairs signed rank test, for selection criteria see Methods) and were more likely to be activated by the CS+ than the CS- (CS+ 25 ± 3%, CS- 8 ± 1%, P = 0.004, Wilcoxon matched-pairs signed rank test) (**Fig. 5b-d**).

To classify neurons according to the evolution of their CS+ responses upon fear conditioning and extinction, we used a supervised clustering approach (**Extended Data Fig. 4a**, see Methods). Consistent with previous findings[31,33,46–48], we found functionally distinct CS plasticity subtypes of BA PNs that were characterized by differential changes of CS+ responses during fear conditioning and extinction (**Fig. 5b,e**). Fear neurons (29 ± 4% of all CS+-responsive neurons) exhibited increased CS+ responses after fear conditioning which were decreased again upon extinction learning (**Fig. 5b**). In contrast, extinction neurons showed a selective increase in their CS+ responses after fear extinction (14 ± 3%). The CS+ responses of extinction-resistant neurons were enhanced after fear conditioning and remained elevated upon extinction (20 ± 3%). Additionally, we identified neurons which decreased their responses after habituation, CS-down neurons[33] (23 ± 6%) as well as extinction down neurons, which exhibited decreased CS responses after fear extinction (7 ± 1%). Stable neurons (8 ± 3%) showed constant CS responses before and after fear conditioning, as well as after extinction. Interestingly, none of these CS plasticity subtypes were correlated with either of the behavioral state-related neuronal ensembles (**Extended Data Fig. 5a**), indicating that experience-dependent CS representations are maintained across behavioral states.

US responses were dynamic upon fear conditioning (**Fig. 5f**). Across the five CS-US pairings, a supervised cluster analysis (**Extended Data Fig. 4b**) identified different subtypes of US-excited neurons (32 ± 2% of all neurons): US-stable (22 ± 3%), US-down (27 ± 4%), US-up neurons (20 ± 4%) as well as post-US neurons (31 ± 5%), which are off-responsive with peak responses after the end of the US. Additionally, the following subtypes of US-inhibited neurons were identified (25 ± 2%, compared to US-excited: P = 0.129, Wilcoxon matched-pairs signed rank test): stable US-inhibited neurons (74 ± 3%), which show a constant inhibition during the US and plastic US-inhibited down neurons, with a decreasing inhibitory response upon US presentation (26 ± 3%) (**Fig. 5f-h)**. Despite the highly diverse and dynamic response patterns of CS and US responses across the entire population of BA PNs, no significant overlap between individual CS and US plasticity subtypes was observed (**Extended Data Fig. 4c; Extended Data Fig. 5a,c**, see also **Fig. 4**). Notably, a population level analysis revealed that US responses per se were not correlated with any of the tested behavioral states (**Fig. 5i, Extended Data Fig. 5b**), indicating that US representations are not specifically associated with a particular behavioral state. Overall, these results demonstrate that, on the level of BA neuronal populations, sensory representations of the US are orthogonal and uncorrelated with behavioral state-related population activity.

A more detailed analysis of CS+ responses across behavioral paradigms revealed that before fear conditioning and after fear extinction, the population level CS+ response was not correlated with exploratory or freezing behaviors, which is consistent with the neutrality of the CS+ response at these time points. Strikingly though, after fear conditioning, the CS+ population response was weakly correlated with exploratory, low anxiety behaviors (corner entries, freezing end, head dips, **Fig. 5i**). Consistent with this observation, we found that after fear conditioning, more CS+ responsive neurons overlapped with freezing start-inhibited neurons (32 ± 5%, ensemble 1), which are typically activated by exploratory behaviors (**Fig. 4**), than with freezing start activated neurons (18 ± 4%, ensemble 2, Friedman test (P = 0.03, F = 6.89) with *post hoc* Dunn's multiple comparison test, **Fig. 5j,k**, for US see **Extended Data Fig. 5b**). A stronger CS+ representation in freezing-inhibited neurons, separating state-activated ensembles from sensory coding neurons, may respresent a possible circuit mechanism to enhance the signal-to-noise ratio for salient sensory stimuli such as a CS after conditioning.

Finally, given previous reports indicating that defined BA output pathways are involved in specific behaviors[31,32,48–50], we tested the hypothesis that the BA would transmit distinct behavioral state- or sensory-related representations to selected downstream targets including the ventral hippocampus (vHC), the medial prefrontal cortex (mPFC) or the nucleus accumbens (NAc). Although some specialization could be observed for individual

pathways (typically CS/US coding-related[51]), the population correlations with behavioral states was largely maintained across output pathways (**Extended Data Fig. 6**), suggesting that the BA broadcasts state-related signals to larger brain networks.

Discussion

Our study reveals a novel coding principle of state representations in large, functional ensembles of BA neurons (**Extended Data Fig. 7**). We show that behavioral state transitions are associated with inverse dynamics in two functionally distinct, anatomically intermingled ensembles of BA neurons. State-coding in amygdala ensembles was consistent across behavioral paradigms and reflected transitions from exploratory behavior to defensive, anxiety-like states and back. Consistent state-dependent changes in the activity of single cells suggest a fixed state ensemble membership of individual neurons and a homogenous, state-dependent, regulation of individual neuron activity within a given state ensemble. Changes in population activity upon state transitions were characterized by slow (seconds), continuous dynamics in defined ensembles, reminiscent of a potential amygdala attractor network state, which has been previously suggested to underly internal states[52]. Such slow regulation of antagonistic BA ensemble activity might involve state-dependent changes in input activity and local circuit mechanisms[53–56].

Notably, sensory responses were correlated only partially (CS), or not at all (US), with behavioral states. This suggests that fast sensory dynamics and slow state dynamics are orthogonally separated at the level of amygdala networks, which would allow for a continuous population level state-encoding despite flexible single cell representations of sensory inputs[57]. Additionally, biased representations of emotionally salient stimuli in freezing-inhibited neurons might substantially increase signal to noise ratio and enhance the animal's ability to rapidly and reliably select appropriate behavioral reactions when facing danger. Importantly, state signals were largely conserved across major BA output pathways including projections to the vHC, the NAc and the mPFC. Broadcasting of amygdala state signals to larger brain networks including cortical and subcortical areas is likely to play an important role for state-dependent regulation of sensory perception, motivation[58], foraging[35], spatial preference[59], memory formation[60], as well as motor output[22] and autonomic regulation[25], with a potential to broadly set internal drive and generally modify affective states and behaviors.

Acknowledgements

We thank Georg Keller and Daniela Gerosi Erni for virus production (retroAAV.EF1a.GCaMP6f). and V. Jayaraman, R. Kerr, D. Kim, L. Looger, K. Svoboda and the HHMI Janelia GENIE Project for making GCaMP6 available as well as Alla Karpova and David Schaffer who gifted the rAAV2-retro helper (Addgene plasmid # 81070V). We thank Paul Argast and Peter Buchmann for workshop and engineering support. Research was supported by the Swiss National Science Foundation (Core Grant to A.L., Ambizione Fellowship to J.G., SNF Professorship to J.G., Sinergia to B.F.G.), EMBO and Marie Curie Actions (J.G.), NARSAD (Young Investigator Fellowships to S.K. and B.F.G.), Swiss Data Science Center (B.F.G.), DARPA (M.J.S.), NIH (M.J.S), ERC (Advanced Grant, A.L.) and the Novartis Research Foundation.

Competing interest statement

M.J.S. is a scientific co-founder of Inscopix, Inc., which produces the miniature fluorescence microscope used in this study.

Author contribution

J.G. Y.B., and A.L. designed experiments and analysis. J.G., T.L. and S.K. performed experiments. J.G., B.F.G. and M.J.S. established the Ca^{2+} imaging protocol, experiments and image data analysis. Y.B. and J.G. analysed data. J.G., Y.B. and A.L. wrote the paper and all authors edited the paper and commented on the manuscript.

Methods

Animals and viruses: Male C57BL/6J mice (C57BL/6JRccHsd, Envigo) were used throughout the study. Viruses were purchased from Penn Vector Core (AAV2/5.CaMKII.GCaMP6f.WPRE.SV40, titer: 2.49e13/ml) or custom-made in the case of the retrograde AAV[61] (retroAAV.EF1a.GCaMP6f.WPRE, Georg Keller, FMI Vector Core, titer: 3.9e11/ml). rAAV2-retro helper was a gift from Alla Karpova & David Schaffer (Addgene plasmid #81070). rAAV2-retro virus was supplemented with blue non-retrograde polymer microspheres (1:2400, Duke Scientific Corp.) to label injection sites. All animal experiments were performed in accordance with institutional guidelines and permitted by the authorities of the canton Basel-Stadt.

Surgeries: 8-week-old male mice were anesthetized (isoflurane) and placed in a stereotactic frame (Kopf Instruments). 300 nl (retroAAV.EF1a.GCaMP6f, ventral hippocampus, medial prefrontal cortex, nucleus accumbens) or 500 nl (AAV2/5.CamKII.GCaMP6f, BA) virus was injected in the respective target area using a glass pipette connected to a picospritzer during a stereotactic brain surgery under isoflurane anesthesia (1-2%). One week after virus injection the animals underwent a second surgery for gradient index (GRIN) lens implantation. An 800 µm hole was drilled above the BA. Next, a small track was cut through the hole and cortex to aid GRIN lens insertion. A 600 µm GRIN lens (Inscopix) was then slowly advanced into the basal amygdala (-4.4 mm). The GRIN lens was fixed to the scull using light curable glue (Loctite 4305,

Henkel) and the skull sealed with Scotchbond (3M), Vetbond (3M) and dental acrylic (Paladur, Kulzer). A custom made head-bar for animal fixation during miniature microscope mounting was attached. Animals were provided with analgesia (buprenorphine, ropivacaine) and their well-being was monitored throughout the experimental period.

Behavioral paradigm: Animals were single-housed on a 12-hour light cycle and behavioral experiments were performed during the light period. Anxiety tests and fear conditioning were combined in the following manner on seven consecutive days: open field test, elevated plus maze test, habituation 1, habituation 2, fear conditioning, extinction 1, extinction 2. The open field test was performed in a 40 x 40 x 40 cm plastic box with an evenly distributed light intensity of 24 lux. The elevated plus maze was composed of two orthogonal open and closed arms (30 cm) and a center zone (6 cm) elevated at 55 cm above the ground. Mice were allowed to freely explore the open field and elevated plus maze for 10 to 15 min. Habituation and extinction experiments were performed in a 23 cm diameter round plexiglass context. Mice were presented with 5 CS+ and CS- (6 or 12 kHz, counterbalanced) during the habituation sessions and 4 CS- and 12 CS+ during the extinction session. CSs were presented as 27 200 ms pips at a frequency of 1.1 Hz at 75 dB (Tucker Davis Technologies, TDT 78). Fear conditioning was performed in a 26 cm wide square plexiglass context using a Coulbourn shock grid. The CS+ was terminated with a 2 s 0.65 mA AC foot shock 1.1 s after the last pip. Behavioral experiments were performed and recorded using Sort Client (2.7.0), Radiant (2.0.0) and Cineplex (3.4.1) software in combination with the CinePlex and MAP data acquisition systems (all Plexon). Animals were perfused with 4% PFA in PBS at the end of the behavioral experiment and brain slices (150 µm) were cut (vibratome, Leica) and visualized (confocal microscopy, Zeiss LSM700) to verify GRIN lens location and imaging sites. Animals without detectable GCaMP6f expression before baseplate mounting, non-BA imaging locations or amiss retroAAV injection were excluded from the analysis.

Imaging experiments: Freely moving imaging experiments of large populations of amygdala neurons were performed via the implanted GRIN lens using a miniaturized microscope (nVista, V2, nVista HD 2.0.4 Inscopix)[37]. Microscope base plates were glued to the dental acrylic circa one week before the experiment and mice were habituated to the microscope attachment procedure before behavioral experiments. Miniature microscopes were mounted onto the mouse's head right before each behavioral experiment using a custom built mounting station. Images were acquired at 1024x1024 pixels and at a frame rate of 20 Hz. Imaging parameters were set at 20-80% LED intensity (0.4 - 1.7 mW, 473 nm) and a gain of 1-2 depending on GCaMP6f expression levels.

Data analysis: *Behavior:* Behavioral data was manually scored (EPM, head dips; OF, rearing) or automatically tracked using Cineplex Studio and Editor software (Plexon). Freezing was calculated using the 2D motion data and Freezing Analysis plug-in of Editor (Plexon, minimum absence of movement: 2 s, threshold adjusted on a case-by-case basis) combined with additional manual post hoc checks for non-freezing but stationary behaviors (e.g. grooming). Open field test and elevated plus maze 2D location was tracked offline. Open field locations were defined as follows: center: center quarter of open field area, corners: 1/16th of open field area measured from each corner of the arena. Corner entry and exit times were detected as the animal's crossings of the corner area outlines (36 ± 7 transitions / animal) with a minimum time of 0.5 s in each area before and after outline transition to exclude events which were non-directed outline crossings (e.g. lingering on the zone border). The number of corner transitions, EPM closed and open arm as well as center location times were calculated using Editor (Plexon) and Matlab.

Ca^{2+} imaging: Imaging raw movies were pre-processed and normalized using a fast Fourier transform band pass filter in ImageJ. For normalization, each image was divided by its filtered image. After pre-processing, the movies were spatially down-sampled by a factor of four. The movies of all individual experimental days were then concatenated and motion corrected across all frames in Matlab using the TurboReg algorithm[62]. Single cell ROIs were extracted using a combination of principal and independent component analysis[33,63]. ROI size was limited to a maximum diameter of 30 pxl (ca. 60 µm). ROIs were then overlaid with a maximum intensity projection of the raw movie and excluded, if they overlapped with non-cellular components (e.g. edge of GRIN lens, blood vessels) or if multiple ROIs were detected for the same maximum intensity projection of the same neuron. Pixels within ROIs were normalized and cut at 50% of the maximum ROI pixel intensity. Fluorescence traces for each ROI were extracted as average pixel intensity within the normalized ROI along the filtered 20 Hz motion filtered and corrected raw movie. Traces which failed to pass quality criteria upon visual inspection across sessions were excluded.

Prior to further analysis Ca^{2+} traces were calculated as z-scores and linear trends calculated for the entire imaging session were removed.

Area scores: The area bias in single neuron responses was calculated using the average spatial activity map of each neuron: the total activity in a specific x-y location normalized by the total time the animal spent in that location. X-y data was discretized in 256 pixels and smoothed with a 2-d Gaussian kernel that was 1/64 the arena size. The difference between the total normalized activation in the corners (defined as above) and the center was used as a measure of the bias. We calculated the area score for

all neurons in the dataset, and set the threshold as 1 standard deviation around zero, to capture the behavior of the distribution tails. This threshold was fixed for the single animal analysis.

Area decoding: We used support vector classification with a quadratic kernel for all decoders. Animal location was determined in 1-s bins as center/corners/walls according to the definitions above, and bins with non-consistent behavior were excluded from analysis. To avoid very unbalanced designs, if an animal spent less than 15% of the session in the corner, the decoder was trained on the distinction between corner and center. Likewise, if the animal spent less than 15% of the session in the center, the decoder was trained on the distinction between corner and all other locations. In order to control for the local dependencies in both the behavioral data and the neuronal responses, we repeated the decoding training procedure with the behavior circularly rotated relative to the neuronal activity. Maintaining the signal's local structure resulted in a consistent modest drop in decoding performance, that was highly significant (decoding performance on real data was higher than performance on shifted data in 99.8 ± 0.2% of all possible shifts see **Extended Data Fig. 2c**).

Neuronal response analysis and clustering: Behavioral responses to corner entry were averaged for each neuron in a time window starting 2 s before transition to 5 s after. The neuronal responses of all neurons from each animal were then clustered into 3 groups using k-means clustering with Euclidean distance that resulted in an excited, inhibited and neutral cluster for each animal. This procedure was repeated for the responses to the freezing start period (**Fig. 5j**)

CS and US responses were analyzed using a combined statistical and supervised cluster analysis. First, CS and US responsive cells were identified as significantly responsive if their binned Ca^{2+} fluorescence (CS: 1 s bins, ±30 s window around CS onset; US 1 s bin, ±14 s window around US onset) during the stimulus was significantly increased (CS) as well as significantly increased or decreased (US), Wilcoxon Signed Rank test, alpha-level: 0.01) compared to baseline conditions in at least 3 or 2 stimulus presentations for the US or CS, respectively (on at least one experimental condition for CS-responses). This minimum number of stimulus criterion allowed a reliable detection of CS and US plastic neurons compared to a grand average across all stimuli, without being too sensitive for random Ca^{2+} responses in individual trials. Responses for CS were collected to tones 1-5 in the two habituation sessions and in the first extinction session, and to tones 8-12 in the second fear extinction session. The average neuronal responses across both habituation sessions was used as the habituation response of the cells. Next we used a supervised clustering approach on the subset of significantly responsive cells to identify different subtypes of CS and US responsive neurons. Neuronal responses were collected in time windows of [-2 s 15 s] and [-10 s 30 s] around CS and US onset respectively. Principle component analysis was performed on the concatenated responses to the 5 US in the FC session to identify the dynamics in the US response within this session. Responses were then projected on the first 4 principle components (> 60% variance explained) and K-means clustering performed (k = 11). Clusters were manually characterized as the 6 response types described in the article (**Fig. 5 and Extended Data Fig. 5**). This procedure was replicated for the CS responses after averaging responses to the 5 selected tones in the habituation and extinction sessions as described above, to identify the different dynamics in CS responses along the conditioning paradigm.

Behavioral responses to different behaviors were collected and averaged in the different sessions: corner entry (OF), corner exit (OF), freezing period start and end (habituation, extinction), and head dips (EPM). Response to freezing and corner entry/exit was quantified as the difference between the mean response in the 2 s time window starting 1 s after behavioral onset (response) and the 2 s time window ending 1 s before onset (baseline). Head dips were quantified as the difference between the mean response in the 1s time window starting 0.8 s before behavior detection (response) and the 1 s time window ending 1 s before behavior detection (baseline), due the different dynamics of the behavior. We then calculated the pearson correlation between the neuronal responses to each pair of behaviors for each animal.

Statistics: Statistical analysis was performed with Prism 7 (GraphPad) and Matlab (Mathworks). Normality of the data was not assumed and all tests were non-parametric tests. Results are reported as mean ± sem unless otherwise stated. Box and whisker plots indicate median, interquartile range and the minimum to maximum values of the data distribution. Statistical tests and test statics are mentioned in the text and figure legends. *, ** and *** indicate p-values smaller than 0.05, 0.01 and 0.001, respectively. All data and code will be available upon reasonable request.

References

1. Kennedy, A. *et al.* Internal States and Behavioral Decision-Making: Toward an Integration of Emotion and Cognition. *Cold Spring Harb. Symp. Quant. Biol.* **79,** 199–210 (2014).
2. Blanchard, R. J. *et al.* Behavioral and endocrine change following chronic predatory stress. *Physiol. Behav.* **63,** 561–569 (1998).
3. Lester, L. S. & Fanselow, M. S. Exposure to a cat produces opioid analgesia in rats. *Behav. Neurosci.* **99,** 756–759 (1985).
4. Bakshi, V. P., Alsene, K. M., Roseboom, P. H. & Connors, E. E. Enduring sensorimotor gating abnormalities following predator exposure or

corticotropin-releasing factor in rats: A model for PTSD-like information-processing deficits? *Neuropharmacology* **62,** 737–748 (2012).
5. Adamec, R., Fougere, D. & Risbrough, V. CRF receptor blockade prevents initiation and consolidation of stress effects on affect in the predator stress model of PTSD. *Int. J. Neuropsychopharmacol.* **13,** 747–757 (2010).
6. Rajbhandari, A. K., Baldo, B. A. & Bakshi, V. P. Predator Stress-Induced CRF Release Causes Enduring Sensitization of Basolateral Amygdala Norepinephrine Systems that Promote PTSD-Like Startle Abnormalities. *J. Neurosci.* **35,** 14270–14285 (2015).
7. Adamec, R. E. & Shallow, T. Lasting effects on rodent anxiety of a single exposure to a cat. *Physiol. Behav.* **54,** 101–109 (1993).
8. Blanchard, R. J. & Blanchard, D. C. Defensive reactions in the albino rat. *Learn. Motiv.* **2,** 351–362 (1971).
9. Anderson, D. J. & Adolphs, R. A framework for studying emotions across species. *Cell* **157,** 187–200 (2014).
10. Allikmets, L. K. Behavioral reactions to electrical stimulation of amygdala in cats. *Neurosci. Transl.* **1,** 119–127 (1967).
11. Panksepp, J. Aggression elicited by electrical stimulation of the hypothalamus in albino rats. *Physiol. Behav.* **6,** 321–329 (1971).
12. Fadok, J. P. *et al.* A competitive inhibitory circuit for selection of active and passive fear responses. *Nature* **542,** 96–99 (2017).
13. Lin, D. *et al.* Functional identification of an aggression locus in the mouse hypothalamus. *Nature* **470,** 221–227 (2011).
14. Betley, J. N. *et al.* Neurons for hunger and thirst transmit a negative-valence teaching signal. *Nature* **521,** 180–185 (2015).
15. Nieh, E. H. *et al.* Inhibitory Input from the Lateral Hypothalamus to the Ventral Tegmental Area Disinhibits Dopamine Neurons and Promotes Behavioral Activation. *Neuron* **90,** 1286–1298 (2016).
16. Douglass, A. M. *et al.* Central amygdala circuits modulate food consumption through a positive-valence mechanism. *Nat. Neurosci.* **20,** 1384–1394 (2017).
17. Jennings, J. H., Rizzi, G., Stamatakis, A. M., Ung, R. L. & Stuber, G. D. The Inhibitory Circuit Achitecture of the Lateral Hypothalamus Orchestrates Feeding. *Science* **341,** 1517–1521 (2013).
18. Salzman, C. D. & Fusi, S. Emotion, cognition, and mental state represenation in Amygdala and Prefrontal Cortex. *Annu. Rev. Neurosci.* **33,** 173–202 (2010).
19. Lovett-Barron, M. *et al.* Ancestral Circuits for the Coordinated Modulation of Brain State. *Cell* **171,** 1411–1423.e17 (2017).
20. Li, Y. *et al.* Neuronal Representation of Social Information in the Medial Amygdala of Awake Behaving Mice. *Cell* **171,** 1176–1190.e17 (2017).
21. Remedios, R. *et al.* Social behaviour shapes hypothalamic neural ensemble representations of conspecific sex. *Nature* **550,** 388–392 (2017).
22. Tovote, P. *et al.* Midbrain circuits for defensive behaviour. *Nature* **534,** 206–212 (2016).
23. Yang, Y. *et al.* Selective synaptic remodeling of amygdalocortical connections associated with fear memory. *Nat. Neurosci.* **19,** 1348–1355 (2016).
24. Krettek, J. E. & Price, J. L. Projections from the amygdaloid complex to the cerebral cortex and thalamus in the rat and cat. *J. Comp. Neurol.* **172,** 687–722 (1977).
25. Stith, R. D., Person, R. J. & Dana, R. C. Effects of hippocampal and amygdalar stimulation on uptake and binding of 3H-hydrocortisone in the hypothalamus of the cat. *J. Neurosci. Res.* **2,** 317–322 (1976).
26. Rogan, M. T., Stäubli, U. V & LeDoux, J. E. Fear conditioning induces associative long-term potentiation in the amygdala. *Nature* **390,** 604–7 (1997).
27. Belova, M. A., Paton, J. J., Morrison, S. E. & Salzman, C. D. Expectation modulates neural responses to pleasant and aversive stimuli in primate amygdala. *Neuron* **55,** 970–84 (2007).
28. Paton, J. J., Belova, M. A., Morrison, S. E. & Salzman, C. D. The primate amygdala represents the positive and negative value of visual stimuli during learning. *Nature* **439,** 865–70 (2006).
29. Everitt, B. J., Cardinal, R. N., Parkinson, J. A. & Robbins, T. W. Appetitive behavior: impact of amygdala-dependent mechanisms of emotional learning. *Ann. N. Y. Acad. Sci.* **985,** 233–50 (2003).
30. Senn, V. *et al.* Long-range connectivity defines behavioral specificity of amygdala neurons. *Neuron* **81,** 428–437 (2014).
31. Herry, C. *et al.* Switching on and off fear by distinct neuronal circuits. *Nature* **454,** 600–606 (2008).
32. Namburi, P. *et al.* A circuit mechanism for differentiating positive and negative associations. *Nature* **520,** 675–678 (2015).
33. Grewe, B. F. *et al.* Neural ensemble dynamics underlying a long-term associative memory. *Nature* **543,** 670–675 (2017).
34. Lee, S.-C., Amir, A., Haufler, D. & Pare, D. Differential Recruitment of Competing Valence-Related Amygdala Networks during Anxiety. *Neuron* **96,** 81–88.e5 (2017).
35. Amir, A., Lee, S.-C., Headley, D. B., Herzallah, M. M. & Pare, D. Amygdala Signaling during Foraging in a Hazardous Environment. *J. Neurosci.* **35,** 12994–13005 (2015).
36. Likhtik, E., Stujenske, J. M., Topiwala, M. A., Harris, A. Z. & Gordon, J. A. Prefrontal entrainment of amygdala activity signals safety in learned fear and innate anxiety. *Nat. Neurosci.* **17,** 106–13 (2014).

37. Ghosh, K. K. *et al.* Miniaturized integration of a fluorescence microscope. *Nat. Methods* **8,** 871–8 (2011).
38. Lister, R. The use of a plus-maze to measure anxiety in the mouse. *Psychopharmacology (Berl).* **92,** 180–185 (1987).
39. Prut, L. & Belzung, C. The open field as a paradigm to measure the effects of drugs on anxiety-like behaviors: A review. *Eur. J. Pharmacol.* **463,** 3–33 (2003).
40. Botta, P. *et al.* Regulating anxiety with extrasynaptic inhibition. *Nat. Neurosci.* **18,** 1493–1500 (2015).
41. Tye, K. M. *et al.* Amygdala circuitry mediating reversible and bidirectional control of anxiety. *Nature* **471,** 358–62 (2011).
42. Anderson, D. C., Crowell, C., Koehn, D. & Lupo, J. V. Different intensities of unsignalled inescapable shock treatments as determinants of non-shock-motivated open field behavior: A resolution of disparate results. *Physiol. Behav.* **17,** 391–394 (1976).
43. Lee, E. H. Y., Tsai, M. J. & Chai, C. Y. Stress selectively influences center region activity of mice in an open field. *Physiol. Behav.* **37,** 659–662 (1986).
44. Simon, P., Dupuis, R. & Costentin, J. Thigmotaxis as an index of anxiety in mice. Influence of dopaminergic transmissions. *Behav. Brain Res.* **61,** 59–64 (1994).
45. Dalvi, A. & Rodgers, R. J. Behavioral effects of diazepam in the murine plus-maze: Flumazenil antagonism of enhanced head dipping but not the disinhibition of open-arm avoidance. *Pharmacol. Biochem. Behav.* **62,** 727–734 (1999).
46. Amano, T., Duvarci, S., Popa, D. & Paré, D. The fear circuit revisited: contributions of the basal amygdala nuclei to conditioned fear. *J. Neurosci.* **31,** 15481–9 (2011).
47. Quirk, G. J., Repa, J. C. & LeDoux, J. E. Fear conditioning enhances short-latency auditory responses of lateral amygdala neurons: Parallel recordings in the freely behaving rat. *Neuron* **15,** 1029–1039 (1995).
48. Senn, V. *et al.* Long-Range Connectivity Defines Behavioral Specificity of Amygdala Neurons. *Neuron* **81,** 428–437 (2014).
49. Nieh, E. H., Kim, S.-Y., Namburi, P. & Tye, K. M. Optogenetic dissection of neural circuits underlying emotional valence and motivated behaviors. *Brain Res.* **1511,** 73–92 (2013).
50. Felix-Ortiz, A. C. & Tye, K. M. Amygdala Inputs to the Ventral Hippocampus Bidirectionally Modulate Social Behavior. *J. Neurosci.* **34,** 586–595 (2014).
51. Beyeler, A. *et al.* Divergent Routing of Positive and Negative Information from the Amygdala during Memory Retrieval. *Neuron* **90,** 348–361 (2016).
52. Salzman, C. D. & Fusi, S. Emotion, cognition, and mental state representation in amygdala and prefrontal cortex. *Annu. Rev. Neurosci.* **33,** 173–202 (2010).
53. Vogel, E., Krabbe, S., Gründemann, J., Wamsteeker Cusulin, J. I. & Lüthi, A. Projection-Specific Dynamic Regulation of Inhibition in Amygdala Micro-Circuits. *Neuron* **91,** 644–651 (2016).
54. Machens, C. K., Romo, R. & Brody, C. D. Flexible control of mutual inhibition. *Science* **307,** 1121–4 (2005).
55. Kim, J., Pignatelli, M., Xu, S., Itohara, S. & Tonegawa, S. Antagonistic negative and positive neurons of the basolateral amygdala. *Nat. Neurosci.* **19,** 1636–1646 (2016).
56. Amir, A., Headley, D. B., Lee, S.-C., Haufler, D. & Paré, D. Vigilance-Associated Gamma Oscillations Coordinate the Ensemble Activity of Basolateral Amygdala Neurons. *Neuron* **97,** 656–669.e7 (2018).
57. Druckmann, S. & Chklovskii, D. B. Neuronal circuits underlying persistent representations despite time varying activity. *Curr. Biol.* **22,** 2095–2103 (2012).
58. Tye, K. M. & Janak, P. H. Amygdala neurons differentially encode motivation and reinforcement. *J. Neurosci.* **27,** 3937–45 (2007).
59. Felix-Ortiz, A. C. *et al.* BLA to vHPC inputs modulate anxiety-related behaviors. *Neuron* **79,** 658–64 (2013).
60. Paz, R., Pelletier, J. G., Bauer, E. P. & Paré, D. Emotional enhancement of memory via amygdala-driven facilitation of rhinal interactions. *Nat. Neurosci.* **9,** 1321–1329 (2006).
61. Tervo, D. G. R. *et al.* A Designer AAV Variant Permits Efficient Retrograde Access to Projection Neurons. *Neuron* **92,** 372–382 (2016).
62. Thévenaz, P., Ruttimann, U. E. & Unser, M. A pyramid approach to subpixel registration based on intensity. *IEEE Trans. Image Process.* **7,** 27–41 (1998).
63. Mukamel, E., Nimmerjahn, A. & Schnitzer, M. Automated analysis of cellular signals from large-scale calcium imaging data. *Neuron* **63,** 747–760 (2009).

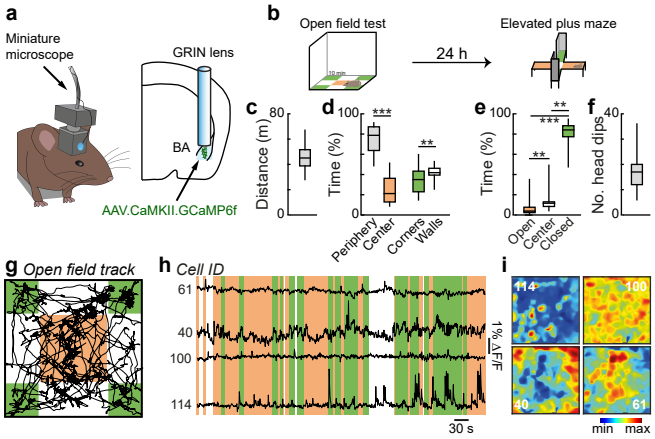

Figure 1: Deep brain imaging of BA activity in freely exploring mice.

a) Scheme of gradient refractive index lens implantation and virus expression strategy. **b**) Scheme of two-day consecutive open field test and elevated plus maze test paradigms. **c**) Distance travelled in open field (N = 25 mice). **d**) Time-spent in center vs. periphery and in subareas of the periphery: walls vs. corners (N = 25 mice). For definition of locations see g. **e**) Elevated plus maze: Time-spent in open and closed arms as well as center. **f**) Average number of head dips on the elevated plus maze (N = 25 mice). **g**) Example open field track of an individual mouse. Context size: 40x40 cm. **h**) Example Ca^{2+} signals of four simultaneously recorded individual cells during open field exploration. Colors indicate mouse location: orange - center, green - corner. **i**) Mean Ca^{2+} signal across the open field arena for the four example cells shown in h demonstrating unspecific (cell 114 and 100) and area-modulated activity patterns (cell 40 and 61). Color bar indicates normalized z-score. Box and whisker plots indicate median, interquartile range and the minimum to maximum values of the data distribution.

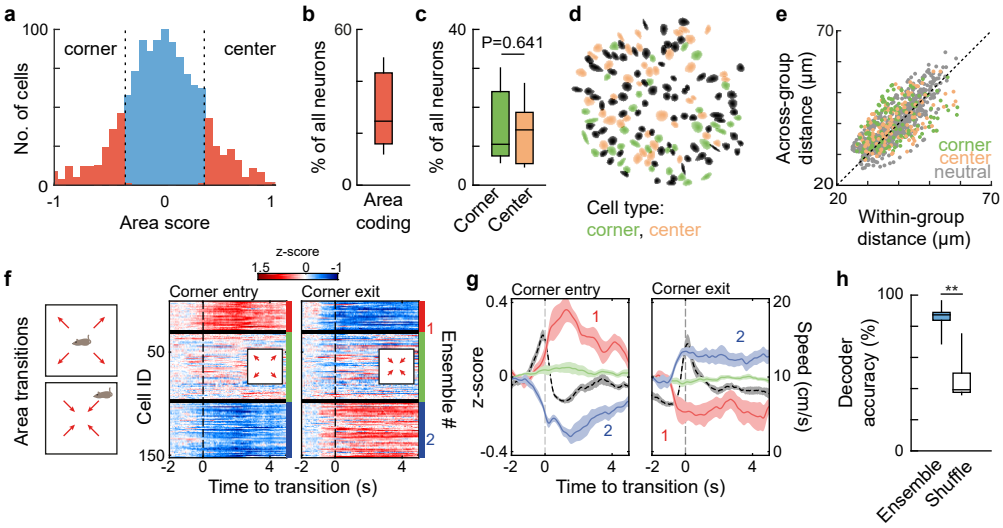

Figure 2: Large, intermingled populations of basal amygdala neurons are spatially modulated. **a**) Histogram of area scores of CaMKII-positive amygdala projection neurons (n = 1201 neurons from 9 mice). Cut-off scores for corner- and center-modulated cells were set at ± 1 standard deviation (vertical dashed lines). **b**) Proportion of area coding neurons. **c**) Proportion of corner- and center-modulated neurons is similar (P = 0.6406, Wilcoxon matched-pairs signed rank test). **d**) Spatial distribution of corner- (green) and center- modulated (red) cells in the BA of one example mouse. Black: neutral cells. **e**) Within- and across-group distance of corner- and center-modulated cells (see also Extended Data Fig. 2b). **f**) Example neuronal responses of functionally clustered groups of neurons upon corner entry (middle) and corner exit (right) transitions (n = 152 simultaneously imaged neurons from one mouse). Zero marks corner entry or corner exit times, respectively (see methods) and responses were baselined using the first 0.5 s response (starting 2 s before transition). K-means clustering was performed on the average corner entry response of each cell and cell IDs were kept identical for average corner exit responses. **g**) Average corner entry (left) and exit (right) response of corner entry activated (red, ensemble 1), neutral (green) or inhibited (blue, ensemble 2) clusters across animals. Black traces indicate the average speed profile upon corner entry or exit. Lines indicate average response across animals ± s.e.m.. As in the example animal shown in g, cluster IDs were based on corner entry responses and kept for corner exits. **h**) Spatial decoding accuracy of corner and center location in actual and time-shuffled data (P = 0.004, Wilcoxon matched-pairs signed rank test). Box and whisker plots indicate median, interquartile range and the minimum to maximum values of the data distribution. All data is generated from N = 9 animals.

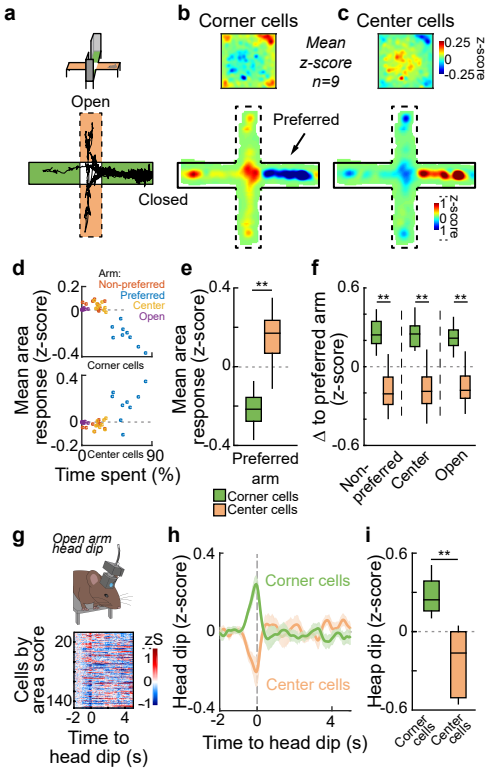

Figure 3: Corner- and center-modulated cells encode exploratory behavior.

a) Open field behavior of the example animal shown in Figure 1. Green areas represent closed arms and orange areas represent open arms of the elevated plus maze. **b**) Average spatial Ca^{2+} activity map of open field corner cells in the open field (top) and on the EPM (bottom) across animals. **c**) Average spatial Ca^{2+} activity map of open center corner cells in the open field (top) and on the EPM (bottom) across animals. Animals typically have a preferred closed arm and EPM maps were rotated such that the most frequented closed arm is aligned on the right (arrow in c). **d**) Mean area responses of all animals in the preferred closed arm, non-preferred closed arm, EPM center and open arms for corner (top) and center (bottom) cells reveals an inverse spatial activity pattern on the elevated plus maze for the two functional cell types. **e**) Average preferred arm response of corner and center cells ($P < 0.01$, Wilcoxon matched-pairs signed rank test). **f**) Response difference of non-preferred arms, open arms as well as center to the preferred, home base arm for corner- and center-modulated cells ($P < 0.01$ for all comparisons, Wilcoxon matched-pairs signed rank test). **g**) Illustration of head dip behavior on EPM open arms (top) and example BA responses to head dips for 152 simultaneously recorded cells of one animal (bottom). Cell IDs sorted by area score (see also Fig. 2a). **h**) Average response of corner- and center-modulated cells upon EPM head dips. **i**) Quantification of peak response shown in h ($P < 0.01$, Wilcoxon matched-pairs signed rank test). Box and whisker plots indicate median, interquartile range and the minimum to maximum values of the data distribution. All data is generated from N = 9 animals.

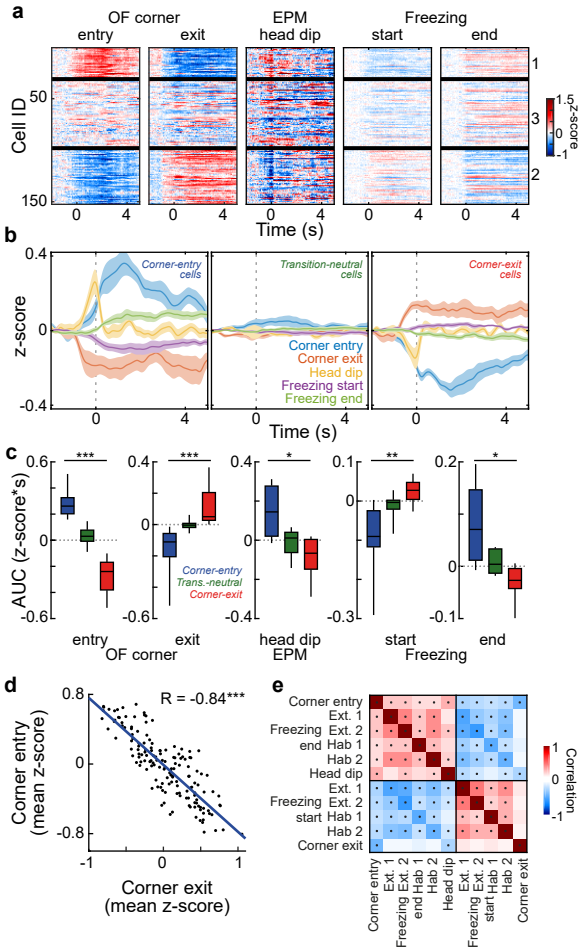

Figure 4: State-coding of BA neuronal ensembles across behavioral paradigms.
a) Average response patterns of open field corner entry, corner exit EPM head dips and freezing start as well as freezing end for cells clustered based on OF corner entry responses (top). **b**) Average cluster response across animals (N = 9). **c**) Quantification of the average cluster responses of open field corner entry (z-score: Corner-entry cells (Ensemble 1) = 0.28 ± 0.04, Transition-neutral cells (Ensemble 3) = 0.03 ± 0.02, Corner-exit cells (Ensemble 2) = -0.27 ± 0.05, P < 0.001 for Corner-entry cells vs. Transition-neutral cells), corner exit (Corner-entry cells = -0.16 ± 0.05, Transition-neutral cells = -0.003 ± 0.01, Corner-exit cells = 0.11 ± 0.04, P < 0.001 for Corner-entry cells vs. Transition-neutral cells), EPM head dips (Corner-entry cells = 0.15 ± 0.04, Transition-neutral cells = -0.01 ± 0.02, Corner-exit cells = -0.09 ± 0.03, P = 0.014 for Corner-entry cells vs. Corner-exit cells) as well as freezing start (Corner-entry cells = -0.09 ± 0.03, Transition-neutral cells = -0.01 ± 0.01, Corner-exit cells = 0.03 ± 0.01, P = 0.003) and freezing end (Corner-entry cells = 0.08 ± 0.02, Transition-neutral cells =0.01 ± 0.01, Corner-exit cells = -0.03 ± 0.01, P = 0.020, all Friedman test with Dunn's multiple comparison test). **d**) Single cell correlation of corner entry and corner exit responses of one example animal (N = 152 cells, R = -0.84, P < 0.001). **e**) Average correlation matrix of single cell responses across different behavioral paradigms (dots indicate a significant difference of the correlation from 0 across animals, one sample t-test). Box and whisker plots indicate median, interquartile range and the minimum to maximum values of the data distribution. All data is generated from N = 9 animals.

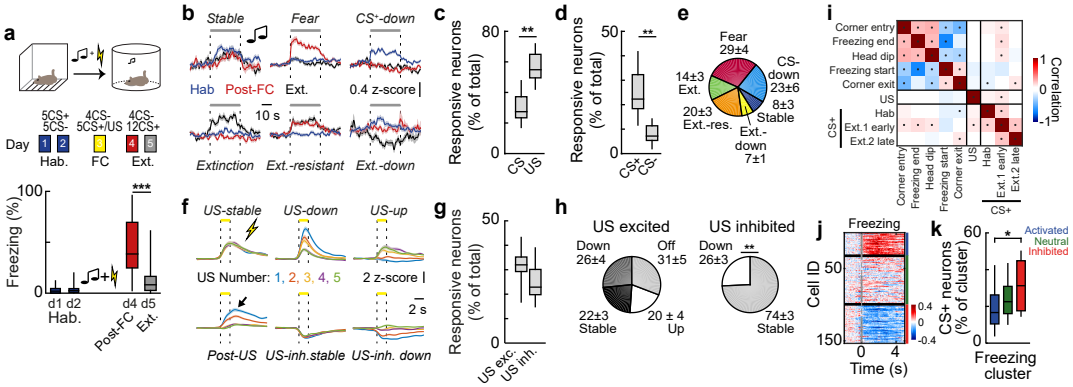

Figure 5: Orthogonal representation of sensory stimuli and behavioral states.

a) Auditory fear conditioning paradigm and average CS+ freezing (Post FC freezing: 44 ± 6 %, post extinction freezing: 13 ± 3 %, P < 0.001, Wilcoxon matched-pairs signed rank test). **b**) Average CS+ responses of stable, fear, CS-down, extinction (Ext.) extinction-resistant (Ext. resistant) and extinction depontiated (Ext. down) neurons. **c**) Proportion of CS and US responsive neurons across animals. **d**) Proportion of CS+ and CS- responsive neurons. **e**) Proportion of subgroups of CS plastic neurons. **f**) Average CS+ responses of stable, fear, CS-down, extinction (Ext.) extinction-resistant (Ext. resistant) and extinction-depotentiated (Ext. down) neurons. **g**) Proportion of US excited and US inhibited neurons across animals (N = 9 animals, P = 0.129, Test = Wilcoxon matched-pairs signed rank test). **h**) Proportion of subgroups of US excited und US inhibited groups. **i**) Single cell correlation matrix of behavioral as well as CS and US responses across animals (dots indicate significant correlations across animals). **j**) Clustered freezing responses of one example animal. Color bar indicates z-score. **k**) Average proportion of CS+ and freezing cluster-responsive neurons out of the total population (CS+ / freezing activated = 18 ± 4 %, CS+ / freezing neutral = 24 ± 3 %, CS+ / freezing inhibited = 32 ± 5 %, P(activated vs. inhibited) = 0.029, Friedman test (P = 0.03, F = 6.89) with post hoc Dunn's multiple comparison test). Box and whisker plots indicate median, interquartile range and the minimum to maximum values of the data distribution. All data is generated from N = 9 animals.

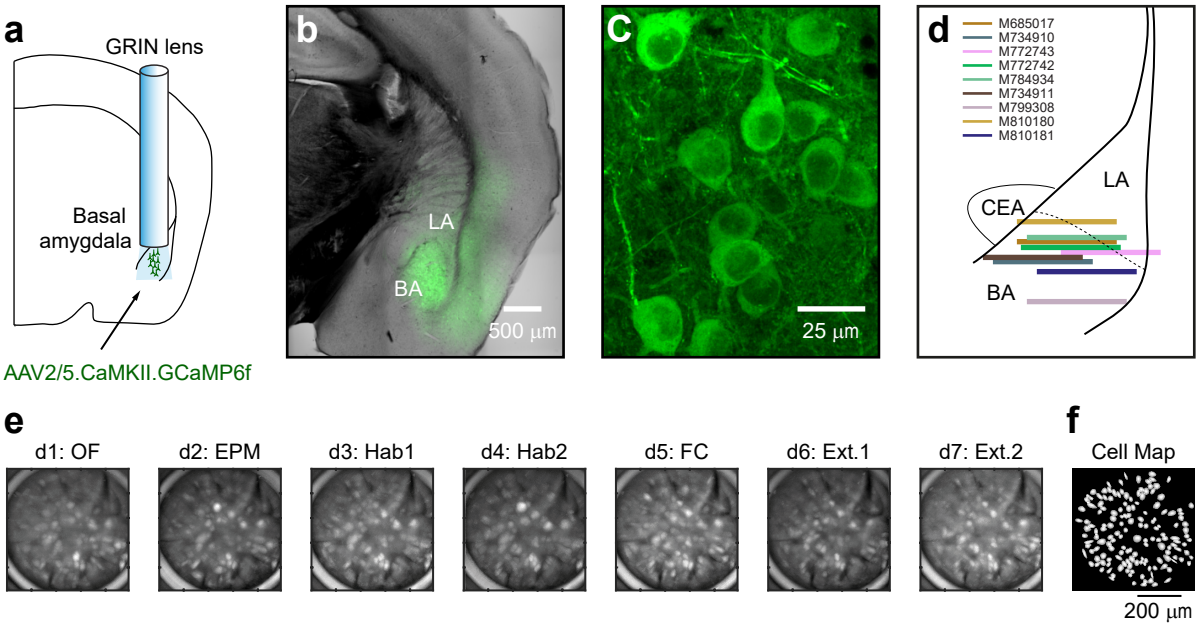

Extended Data Fig. 1: Deep brain imaging of basal amygdala neurons in freely moving animals.
a) Anatomical scheme of virus injection and GRIN lens location. **b**) Anatomical overview (transmission PMT) of GCaMP6f expression (green) in basal amygdala neurons. **c**) Individual basal amygdala neurons expressing GCaMP6f (maximum intensity projection). **d**) GRIN lens front location of animals expressing GCaMP6f non-specifically in large populations of basal amygdala neurons under the control of the CaMKII promotor (N = 9 mice). **e**) Aligned miniature microscope field of view across seven recording days. OF: open field test. EPM: elevated plus maze test. Hab1/2: habituation day 1/2. FC: fear conditioning day. Ext. 1/2: Extinction training day 1/2. **f**) Map of identified cell regions of interest (ROI). ROIs were identified based on the aligned concatenated imaging movies across all experimental days.

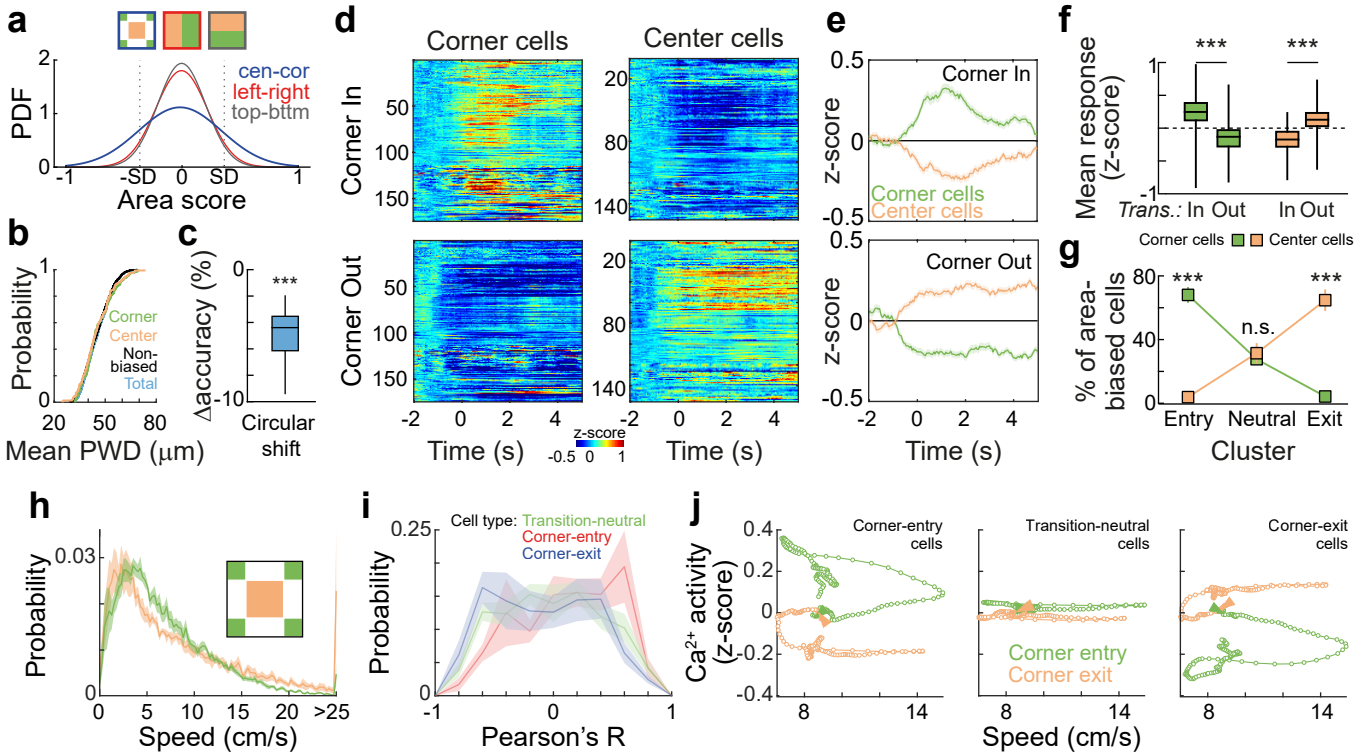

Extended Data Fig. 2. Corner and center cell location, responses upon area transition and speed correlations.

a) Probability density function (Gaussian fit) of area scores based on differential activity in centers vs. corners (cen-cor, blue) as well as neutral devision of the open field (left-right, red; top-bottom, grey, n = 1201 cells out of N = 9 animals). plotted SD = standard deviation of cor-cen. SD(cor-cen) = 0.36, SD(left-right) = 0.22, SD(top-bttm) = 0.21, SD(left-right) = 0.22, Brown-Forsythe Test: F = 177.4, P < 0.001. **b)** Cumulative probability distribution of the mean cellular pairwise distance of all corner cells, center cells, non-area-biased cells and the total cell population reveals that the three cell groups are not spatially clustered (Corner vs. total: P = 0.299, Center vs. total: P = 0.414, Non-biased vs. total: P = 0.276, Kolmogorov-Smirnov test). **c)** Average change in deocder accuracy (-5.0 ± 0.7 %) upon circular temporal shift of neuronal activity (N = 9 animals, P = 0.001, One sample T-Test. **d)** Response profile of all corner and center cells upon in corner and out corner transitions. **e**) Average corner (green) and center (orange) cell responses to in corner (top) and out corner (bottom) transitions (mean ± s.e.m of all corner and center cells) . **f**) Average corner and center cell response to transitions in and out of the corner (Corner cell: In = 0.25 ± 0.02 z-score, Out: -0.16 ± 0.02 z-score, P < 0.0001, N = 174 cells; Center cell: In = -0.18 ± 0.01 z-score, Out: 0.15 ± 0.01 z-score, P < 0.0001, N = 155, Wilcoxon matched-pairs signed rank test). **g**) Distribution of corner and center cells across different clusters basend on in corner transitions (N = 9 animals, Corner entry cluster: Corner vs. Center cells: P < 0.001, Transition neutral cluster: Corner vs. Center cells: P = 0.927, Corner exit cluster: Corner vs. Center cells: P < 0.001, Test: 2-way ANOVA with Sidak's multiple comparisons post hoc test). **h**) Distribution of animal speed in the corners and center of the open field arena (mean ± s.e.m distributions of N = 9 animals). **i**) Distribution of individual cell speed correlation Rs based on corner entry response clusters 1, 2 and 3 (mean ± s.e.m distributions of N = 9 animals.). **j**) Ca^{2+} activity in relation to corner entry (green) and corner exit (orange) transition speed for the three response clusters 1,2,3 (average response profile for N = 9 animals) reveals that the relationship between instantaneous speed and cellular activity depends on the spatial destination and is not solely speed-driven. Triangles mark the start of the transition.

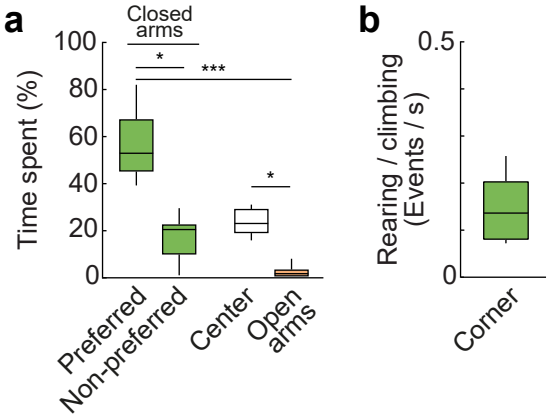

Extended Data Fig. 3. EPM and open field behavior.
a) Average time spent in the preferred (57 ± 5%) and non-preferred (17 ± 3%) closed arms as well as center (24 ± 2%) of the EPM and its open (3 ± 1%) arms. Statistically significant p-values: preferred closed vs. non-preferred closed: P = 0.012, preferred closed vs. open: P < 0.001, center vs. open: P = 0.012. Friedman test with *post hoc* Dunn's multiple comparisons test. **b**) Average time-normalized rearing and climbing events in OF corners (0.14 ± 0.02 events/s).

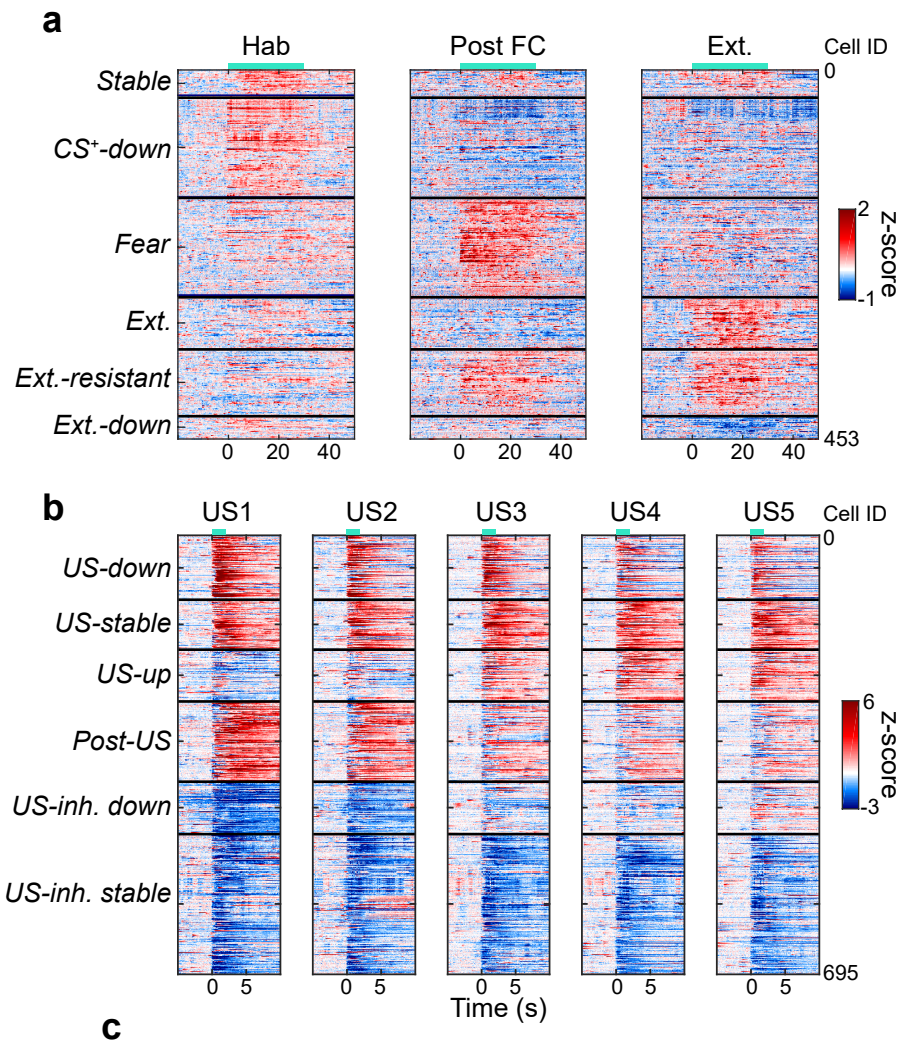

c

CS \ US	Down	Stable	Up	Post	Inh. down	Inh. stable	Non.-sig.
Stable	1	2	1	0	4	3	12
Down	6	4	8	9	7	12	32
Fear	8	8	6	7	7	15	30
Ext.	8	1	3	4	5	7	16
Ext. resistant	3	4	3	4	7	15	19
Ext. down	4	2	1	1	0	4	7
Non-sig.	72	58	60	102	53	166	390

Extended Data Fig. 4. Clusters of CS and US responses.
a) Average CS+ Ca^{2+} signal of all tone-responsive basal amygdala neurons on three different experimental days. Left: Average response of 10 CS+ responses during habituation day 1 and 2. Middle: Average of the first 5 CS+ responses post fear conditioning on extinction day 1. Right: Average of the last 5 CS+ responses after fear extinction on extinction day 2 (n = 453 neurons from 9 animals). **b**) US Ca^{2+} signal of all shock-responsive basolateral amygdala neurons during fear conditioning. US1-5 indicate the five consecutive USs during tone-shock pairings (n = 695 neurons from 9 mice). Horizontal black lines indicate the cluster borders between the different plasticity types of tone- or shock-responsive neurons, respectively. Horizontal turquois lines indicate start of the CS (tone pips) or US, respectively. **c**) Total number of intersected functional classes of CS+ and US responsive neurons (data from 9 mice, P = 0.4336, Chi-square test).

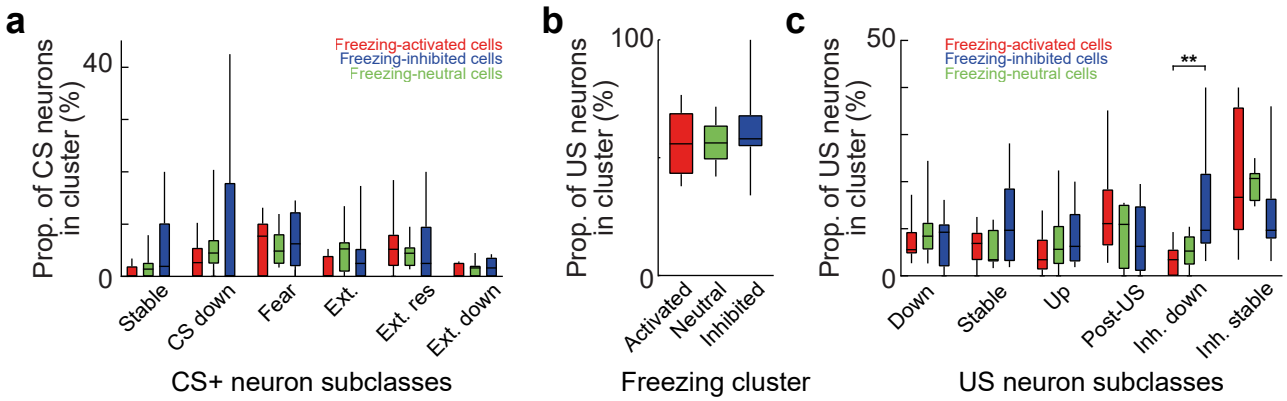

Extended Data Fig. 5. Overlap of CS / US and freezing coding subgroups.
a) Average proportion of CS+ coding subgroups in freezing activated (cluster 1), freezing neutral, cluster 2 and freezing inhibited neurons (cluster 3). No significant difference in the proportion of CS+ coding subgroups in the three freezing subgroups could be found (Stable: P = 0.532, CS down: P = 0.547, Fear: P > 0.999, Ext.: P = 0.475, Ext. resistant: P = 0.685, Ext. down: P = 0.784, Friedman test). **b**) Proportion of general US-responsive neurons in freezing- up, neutral and down-regulated neurons (P = 0.187, Friedman test). **c**) Average proportion of US coding subgroups in freezing activated (cluster 1), freezing neutral (cluster 2) and freezing inhibited neurons (cluster 3). No significant difference in the proportion of US coding subgroups in the three freezing subgroups could be found (Down: P = 0.569, Stable: P = 0.569, Up: P = 0.654, Post-US: P = 0.741, Inh. down: P = 0.007, Dunn's multiple comparisons test: Cluster 1 vs. Cluster 2: P = 0.0096, Inh.: P = 0.057, all Friedman test). Box and whisker plots indicate median, interquartile range and the minimum to maximum values of the data distribution. All data is generated from N = 9 animals.

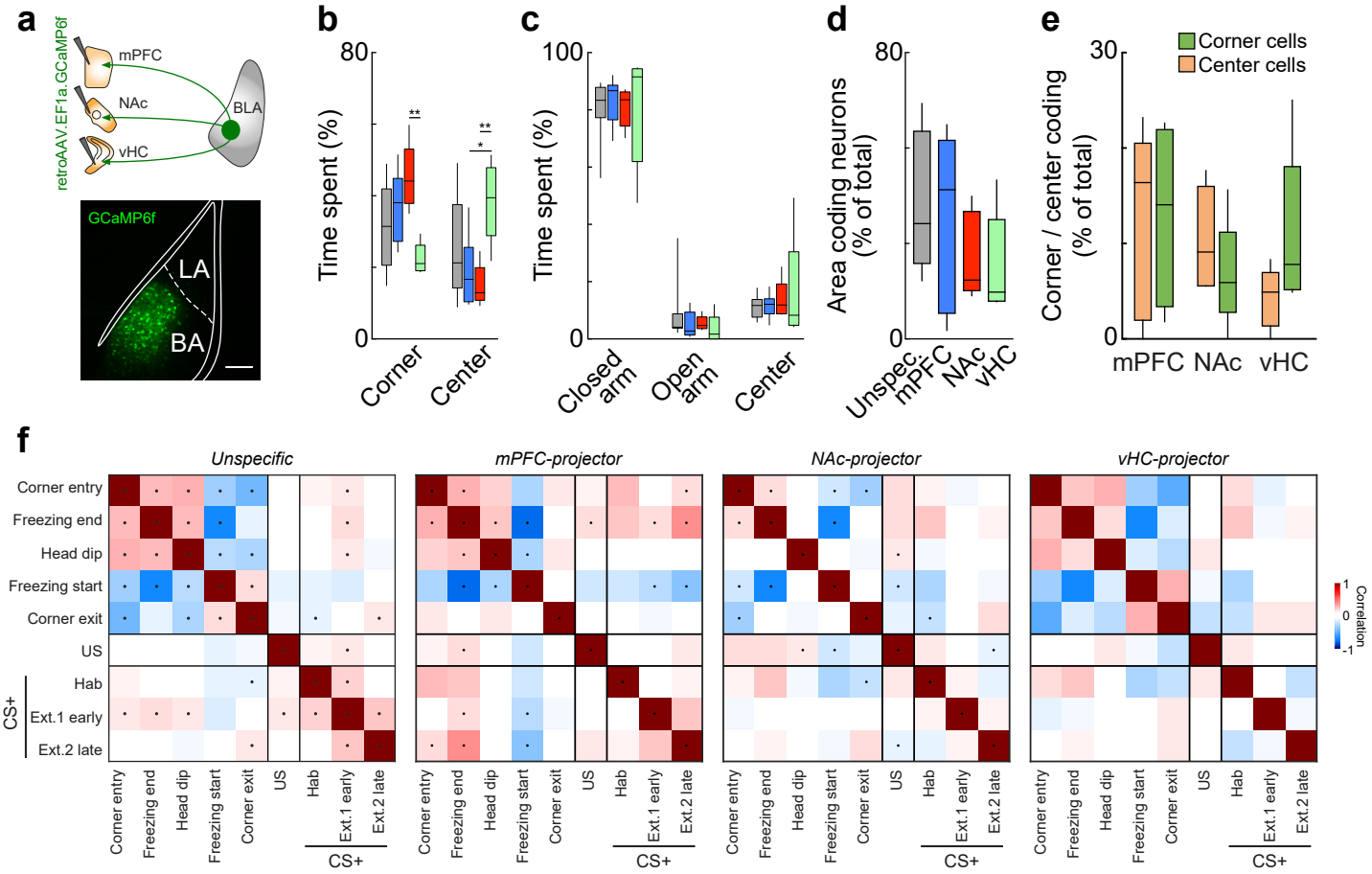

Extended Data Fig. 6. Area spefic coding and neuronal population correlations across behavior and sensory representations of defined basal amygdala projection neurons.
a) Viral strategy for retrograde AAV labelling of amygdala projection neurons with GCaMP6f. GCaMP6f expression in mPFC-projecting BA neurons. Scale bar: 200 μm. **b**) Summary data of open field behavior in unspecific and projection neuron groups. Corner NAc vs. Corner vHC: P = 0.0071, Corner mPFC vs. Corner vHC: P = 0.017, Corner NAc vs. Corner vHC: P = 0.005, Two-way ANOVA, Tukey multiple comparison. **c**) Summary data of elevated plus maze behavior for unspecific and projection neuron groups. Two-way ANOVA, Tukey multiple comparison. No difference between projector groups. **d**) Summary data of area-biased neurons for all groups. P = 0.255, Kruskal-Wallis test. **e**) Summary of corner and center cell proportions in projection neurons. No significant difference between groups. Wilcoxon matched-pairs signed rank test. **f**) Correlation matrices of population responses during exploratory and freezing behavior as well as CS and US responses for unspecific neurons, mPFC-projectors, NAc-projectors and vHC-projectors. Box and whisker plots indicate median, interquartile range and the minimum to maximum values of the data distribution. All data is generated from the following number of animals: unspecific: 9, mPFC: 6, NAc: 5, vHC: 5 (except panel f: vHC = 4).

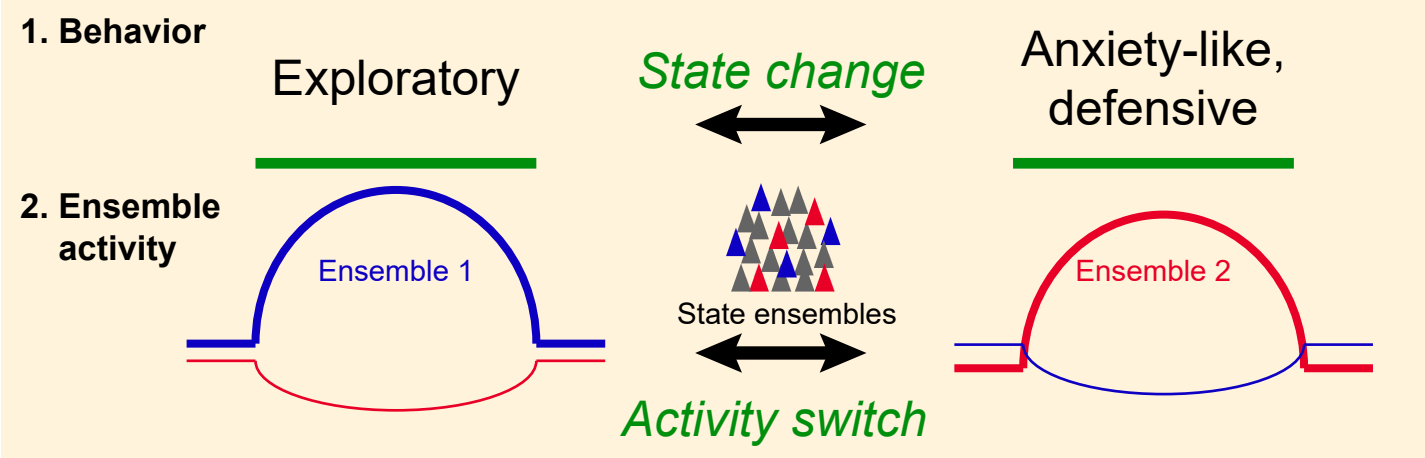

Extended Data Fig. 7: Two large, non-overlapping amygdala populations encode beavioral states.
State changes from exploratory, low anxiety behaviors (e.g. corner behavior, exploration in the open field, head dips, reduction of freezing) to increased anxiety, defensive behaviors (e.g. center behavior, homebase arm retreat, start of freezing) are encoded by two, opposingly activated, non-overlapping ensembles of basal amygdala principal neurons. This ensemble activity signature is recurring across different behaviors associated with the same state, and switches sign when the animal enters an antagonistic state.